



Cite this: DOI: 10.1039/d0ce00638f

Received 28th April 2020,
Accepted 29th June 2020

DOI: 10.1039/d0ce00638f

rsc.li/crystengcomm

Mechanochemical approaches towards the *in situ* confinement of 5-FU anti-cancer drug within MIL-100 (Fe) metal–organic framework†

Barbara E. Souza  and Jin-Chong Tan *

We elucidate two annealing assisted mechanochemical methods to achieve one-pot encapsulation of anti-cancer drug 5-fluorouracil (5-FU) in the iron-based MIL-100 metal–organic framework (MOF). We compare the structural and physicochemical properties of drug@MIL-100 systems derived from *in situ* manual and vortex grinding, where the former technique exhibits a slower drug release due to stronger guest–host interactions.

There has been a rising interest in the advancement of environmentally and biologically friendly synthesis methods exploiting supramolecular bonds to yield porous frameworks.¹ Notably, metal–organic frameworks (MOFs) have gained significant importance in recent years due to their viability as porous vessels for the creation of bio-oriented guest@MOF composite systems, which hold promise as an effective carrier for the controlled release of various therapeutic molecules.²

A few studies have reported the use of mechanochemistry for the synthesis of MIL-100 (Fe) and other MOFs, where a milling technique has been used to accomplish neat or liquid-assisted grinding to fabricate this porous material.³ The mechanochemical approach can help to mitigate the harsh conditions (*i.e.* high-pressure and -temperature paired with the use of nitric (HNO₃) and hydrofluoric acids (HF)) conventionally applied in the synthesis MIL-100 (Fe), while greatly reducing the use of toxic and costly organic solvents.⁴ The use of these noxious compounds in material synthesis can hinder the prospective bioapplications of this promising host framework.

Although the mechanochemical synthesis of pristine MIL-100 (Fe) material has been demonstrated before, one-pot encapsulation of guest molecules into this Fe-based MOF *via* mechanochemistry is less understood. Specifically, for MOFs such as MIL-100 (Fe) possessing highly accessible coordinatively unsaturated metal sites (CUS) that act as a strong binding site for guest drug molecules, the solvent-free encapsulation method can eliminate the competition drug molecules might face against the polar solvents for the active binding sites.⁵ This is particularly relevant when compared to most commonly applied *ex situ* encapsulation method, based on the immersion of a pre-synthesized (host) MOF into a saturated solution of the (guest) drug for encapsulation by a slow diffusion process.⁶

In this work, we report the detailed fabrication of a drug@MOF composite system using an annealing assisted mechanochemical approach. We compare two different methods (*i.e.* manual grinding (MG) *vs.* automated vortex grinding (VG)) to accomplish the *in situ* encapsulation of the anti-cancer drug: 5-fluorouracil (5-FU), within the pores of the MIL-100 (Fe) host framework, producing the 5-FU@MIL-100 composite systems. Details of the synthetic routes are presented in the ESI.† We demonstrate its feasibility as a facile solvent-free one-pot strategy. We have selected 5-FU, a commercial anti-cancer drug, as a model guest molecule due to its structural characteristics (*i.e.* active polar sites) and its hydrophilic character, preventing it from passing through cell membranes without the aid of a drug delivery system.⁷ Very recently, we have reported *ex situ* drug encapsulation of MIL-100 (Fe), where water-based reconstruction was employed to improve framework crystallinity.⁸ Our manual and vortex grinding strategies were adapted from Stojakovic *et al.*⁹ and Han *et al.*¹⁰ to enable *in situ* drug encapsulation, not yet demonstrated in the former studies.

Fig. 1a–g illustrate the *in situ* encapsulation process. For the manual grinding approach, all reactants (*i.e.* organic linker H₃BTC, iron nitrate, and 5-FU) were manually ground using a mortar and pestle. We have designed and 3D-printed

Multifunctional Materials and Composites (MMC) Laboratory, Department of Engineering Science, University of Oxford, Parks Road, Oxford, OX1 3PJ, UK.
E-mail: jin-chong.tan@eng.ox.ac.uk

† Electronic supplementary information (ESI) available: Materials synthesis methods, materials characterization techniques, INS spectra, electron micrographs, adsorption isotherms, TGA and FTIR spectra. See DOI: 10.1039/d0ce00638f





Fig. 1 *In situ* encapsulation of 5-FU and structural characterization of MIL-100 (Fe) and drug@MOF composites. (a) Schematic representation of the manual grinding process used to fabricate 5-FU@MIL-100_MG. (b) 3D-printed holder designed for the vortex grinding process which was cured under UV light (c) to enhance mechanical properties. (d) A propylene container was inserted into the holder and the assembly (e) was installed on a vortex mixer. (f) 4 mm diameter stainless-steel spheres used for the fabrication of 5-FU@MIL-100_VG as schematically represented in (g). (h) Schematic representation of guest–host interaction of 5-FU to the unsaturated iron sites of MIL-100. (i) PXRD patterns of MIL-100 (Fe) and drug-loaded counterparts. (j) FTIR spectra of MIL-100 (Fe) samples measured in ATR mode. Asterisks mark the position of the 5-FU peaks. Colour scheme: iron in orange, carbon in black, oxygen in red, hydrogen in white, nitrogen in purple, and fluorine in green.

a customized holder to couple a standard polypropylene container to an automatic vortex mixer (Fig. 1b–e). This setup allowed us to apply a higher number of rotations per minute *via* the vortex mixer, increasing the number of collisions induced between the solid reactants and the stainless-steel spheres (Fig. 1f and g).

Fig. 1h shows a schematic representation of the encapsulation of the drug guest molecules, yielding guest–host interaction of 5-FU with the CUS located on the iron trimers of MIL-100 (Fe) host to form the C=O...Fe coordination. Indeed, similar interactions involving organic molecules binding to the CUS of MIL-100 (Fe) have been reported.¹¹ Fig. 1i shows the powder X-ray diffraction (PXRD) patterns of pristine MIL-100 (Fe) and drug@MIL-100 systems, confirming the successful synthesis of crystalline MIL-100 (Fe) through both annealing assisted mechanochemical approaches. The effect of the different synthesis/encapsulation technique on the material crystallinity has been monitored *via* analysis of the PXRD data. The evolution of the relative peak intensity corresponding to the two most intense Bragg peaks [*i.e.* (022):(357) ratio] (Fig. 1i) and the changes in the full width at half maximum (FWHM) of the (022) peak at $2\theta = 4^\circ$ (Fig. S1, ESI†) have been monitored as a function of the grinding technique used. The ratios of the relative intensity of the (022):(357) planes showed consistency across all the samples. There was no significant difference found between the pris-

tine samples of MIL-100 (Fe) MG and MIL-100 (Fe) VG. Similar results were observed in the drug-loaded counterparts. However, further assessment of the samples crystallinity *via* analysis of the FWHM of the (022) peak (Fig. S1a, ESI†) shows that 5-FU@MIL-100_VG and 5-FU@MIL-100_MG present relatively sharper peaks (higher crystallinity) compared with their pristine counterparts. This might be attributed to the role played by 5-FU molecules in the deprotonation of the H₃BTC organic linkers, because the nitrogen atoms of 5-FU are proton acceptor sites (see Fig. S1b†). The PXRD patterns of the MG and VG samples before and after the annealing step are shown in Fig. S2†. The comparison reveals that the mechanical stress from grinding was responsible for the formation of MIL-100 (Fe) structure, while the subsequent heat treatment by annealing only helps to enhance the sample crystallinity. Noteworthy, our result is different from that reported by Kuroda *et al.*¹² who used the annealing step after mechanochemical grinding (of a coordination polymer) to yield a new phase with a different crystalline structure. Conversely, we found the basic structure of MIL-100 (Fe) has remained unaltered after annealing (Fig. S2†).

The attenuated total reflectance Fourier transform infrared (ATR-FTIR) spectra of all the samples are presented in Fig. 1j. The vibrational data allow us to investigate in detail the chemical structure of the samples in the mid-infrared region. The characteristic bands of MIL-100 (Fe) (*i.e.* $\nu(\text{C-H})$ in



the organic linker at 707 cm^{-1} and 760 cm^{-1} , $\nu(\text{O}-\text{C}-\text{O})$ and $\delta(\text{O}-\text{H})$ at 1371 cm^{-1} and 1441 cm^{-1} , and $\nu(\text{C}=\text{O})$ in the carboxylic group at 1623 cm^{-1} ¹³ were detected, confirming retainment of the chemical bond integrity after 5-FU loading by both encapsulation techniques. The spectrum of the unencapsulated 5-FU enables the identification of the drug bands in the drug@MOF systems from experiments and theory (density functional theory calculations) (Fig. S3†). The spectra of 5-FU@MIL-100_MG and 5-FU@MIL-100_VG display changes in the regions of $800\text{--}1300\text{ cm}^{-1}$ and $1680\text{--}1800\text{ cm}^{-1}$, in comparison to the spectrum of pristine MIL-100 (Fe), confirming the presence of drug molecules in the drug@MOF assemblies. However, there are salient differences between the spectra of the two different drug-loaded systems, indicating distinct guest–host interactions resulting from the two encapsulation techniques. In 5-FU@MIL-100_VG spectrum the modes at 945 cm^{-1} , 995 cm^{-1} , and 1140 cm^{-1} associated with $\delta(\text{N}-\text{H})$ and $\nu(\text{C}-\text{N}-\text{H})$, respectively, are evident. In contrast, in the 5-FU@MIL-100_MG spectrum these modes are more suppressed while the vibrations at 810 cm^{-1} , 1210 cm^{-1} , and 1247 cm^{-1} , associated with δ -ring and $\nu(\text{C}-\text{F})$, respectively, are apparent (see Fig. S3 and S4 in the ESI† for details and schematic representation of the vibrational modes). These observations suggest the higher efficacy of the manual grinding encapsulation process towards the successful confinement of 5-FU drug molecules within the MIL-100 (Fe) pores.

The level of guest encapsulation was evaluated by Brunauer–Emmett–Teller (BET) surface area from N_2 adsorption isotherms (Fig. 2a), and further estimated by thermogravimetric analysis (TGA) (Fig. 2b). The surface area of the pristine MIL-100 (Fe)_MG ($793\text{ m}^2\text{ g}^{-1}$) and MIL-100 (Fe)_VG ($753\text{ m}^2\text{ g}^{-1}$) are in good agreement with the values of other reported mechanochemically synthesized MIL-100 (Fe) samples (Table S2, ESI†).^{3b,13,14} We have determined the drug loading in 5-FU@MIL-100_MG and 5-FU@MIL-100_VG to be 20.2 wt% (0.25 g/g MOF) and 18.3 wt% (0.22 g/g MOF), respectively. The BET surface area of the drug@MOF samples was found to be greatly reduced to $333\text{ m}^2\text{ g}^{-1}$ (reduction of $\sim 58\%$) and $697\text{ m}^2\text{ g}^{-1}$ (reduction of $\sim 7.5\%$), respectively. These results further indicate that although the vortex grinding is very effective for the synthesis of pristine MIL-100 (Fe) MG, the manual grinding process appears to be more efficient for the encapsulation of 5-FU within the MOF pores. As indicated by the FTIR vibrational data, we hypothesize that the $\text{C}=\text{O}\cdots\text{Fe}$ coordination strongly limits the displacement of nitrogen atoms, thus suppressing the $\delta(\text{N}-\text{H})$ and $\nu(\text{C}-\text{N}-\text{H})$ modes in 5-FU@MIL-100_MG (Fig. 1j). Conversely, the identification of drug molecule “free” motions in the 5-FU@MIL-100_VG spectrum suggests that 5-FU molecules could be adsorbed onto the external surfaces of the MIL-100 crystals by weaker intermolecular interactions (*e.g.* π - π interactions between 5-FU and BTC linker).

An increase in the thermal stability of 5-FU@MIL-100_MG and 5-FU@MIL-100_VG was observed when compared to MIL-100 (Fe) MG and MIL-100 (Fe) VG samples (see Table S3

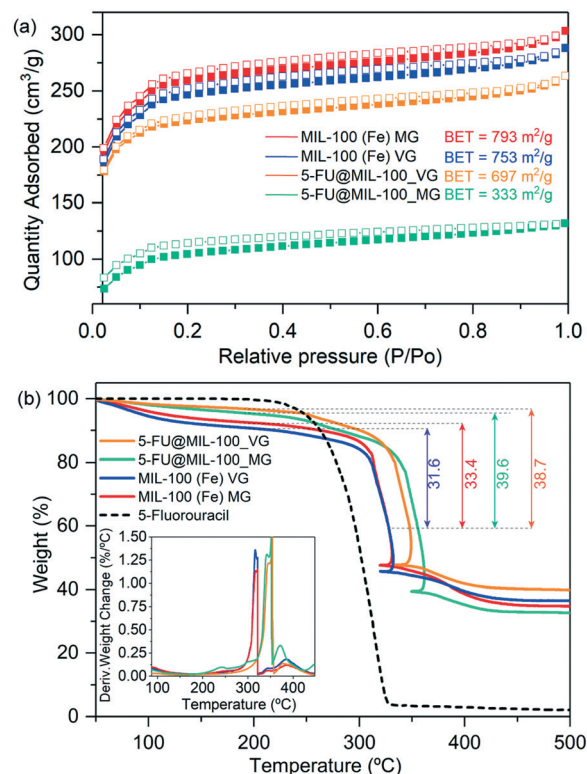


Fig. 2 (a) Nitrogen adsorption (filled symbols) and desorption (empty symbols) isotherms of MIL-100 (Fe) and drug loaded counterparts. The comparison between samples under study shows clear decrease in accessible surface area upon guest encapsulation. (b) TGA plots of MIL-100 (Fe) samples and drug@MOF composites showing material decomposition as a function of increasing temperature. Insets show the derivative weight change with respect to temperature. Note that the decrease of the temperature in the TGA plots over $300\text{ }^{\circ}\text{C}$ is due to highly exothermic process related to the departure of the organic linker, exceeding the set program temperature. The furnace temperature thus decreases in order to follow the initial program temperature.⁶

in the ESI† for further detail). This can be attributed to the improved crystallinity presented by the drug@MOF systems in comparison to their pristine counterparts (see Fig. 1i).

The samples morphology was examined *via* scanning electron microscopy (SEM) as presented in Fig. S5 and S6†. SEM images show no significant changes upon 5-FU loading. The nature of the grinding process appears to favour the formation of fragmented aggregates of MIL-100 (Fe) crystals, which have a non-uniform size distribution (*ca.* $2\text{--}30\text{ }\mu\text{m}$).

Fig. 3 shows results of the drug release study of 5-FU from MIL-100 (Fe), conducted in a phosphate buffered saline (PBS) of pH 7.4 used to simulate physiological conditions. We tracked the evolution of the 266 nm absorption band of 5-FU using UV-vis to construct a calibration curve (Fig. 3a and b) to determine the cumulative release of the drug molecules. Drug release profiles obtained for the drug-loaded samples are presented in Fig. 3c. Interestingly, 5-FU@MIL-100_MG shows a significantly slower release of 5-FU. During the first release stage (initial 5 hours), we detected a drug release of $\sim 60\%$ from the vortex grinding sample in comparison to



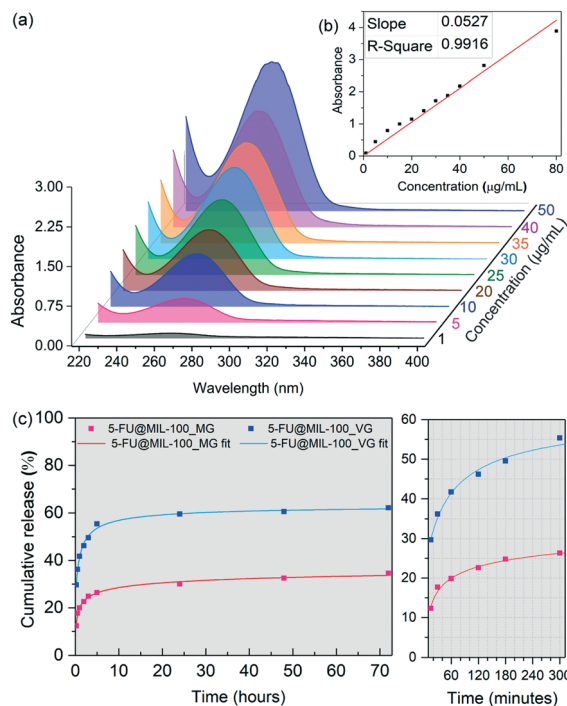


Fig. 3 Drug release studies. (a) UV-vis spectra collected for 5-FU solutions at different concentrations, highlighting the 5-FU band at 266 nm used to establish the calibration curve presented in (b). The calibration equation was used to transform the UV-vis absorbance into the cumulative drug release. (c) Drug release profiles of 5-FU@MIL-100_MG (red trace fit) and 5-FU@MIL-100_VG (blue trace fit) revealing the cumulative release over a period of 72 hours.

~26% released from the manual grinding counterpart. The percentages were calculated by considering the total loading of the drug in the drug@MOF systems, determined by TGA. The second release stage (*i.e.* up to 72 hours) happened in a considerably slower fashion, which stabilizes after 48 hours. 62% and 34% of the 5-FU loaded into 5-FU@MIL-100_VG and 5-FU@MIL-100_MG were released, respectively. Fitted curves of the release profiles revealed that the release process follows a generalized hyperbolic curve for both samples (see Table S4 in ESI† for further details). We assessed the stability of the host framework during the release experiments (Fig. S7 and S8†) to ensure the ongoing stability of the host material during the release of the guest molecules. UV-vis spectra of the supernatant of MIL-100 (Fe) in PBS (Fig. S8†) show no changes in the absorbance bands associated with the MIL-100 host during the drug release measurement. Likewise, PXRD patterns of the host collected after the release experiment (Fig. S7a†) display no signs of MIL-100 (Fe) degradation. The FWHM measured before and after the release process (Fig. S7b†) shows a slight broadening of the (022) peak. However, no evidence of amorphization was found.

The data from the 5-FU drug release study indicate that the manual grinding technique provides a more effective nanoconfinement of 5-FU within the pores of MIL-100 (Fe), while the vortex grinding approach appears to yield weaker guest–host interactions due to adsorption of guest molecules

outside the cages of the host framework. Specifically, this explains the large difference in the amount released in the first hour (doubling that of the vortex ground sample). A slower diffusion at the molecular level throughout the pores is usually associated with strong guest–host interactions.⁶ Consequently, the slower release kinetics of 5-FU from 5-FU@MIL-100_MG indicates stronger guest–host interactions, further supporting the notion that the 5-FU molecules are bound to the CUS through C=O...Fe coordination. The conditions for the establishment of such strong coordination seem to be favoured by the continuous and homogenous grinding provided by the manual grinding approach but disfavoured by the localized collisions that occur during the vortex grinding process (see ESI† for further discussion, section 3.8).

In summary, we have demonstrated that mechanochemistry offers new opportunities for the fabrication of complex MOFs such as MIL-100, and more specifically it is a promising strategy for the nanoconfinement of guest drug molecules within the MOF porosity. By leveraging two annealing assisted mechanochemical based techniques (*i.e.* manual and vortex grinding) for the encapsulation of 5-FU anti-cancer drug in MIL-100 (Fe), we show modifications in the vibrational behaviour of each drug@MOF assembly, revealing the underpinning intermolecular interactions arising from each encapsulation technique. The outcomes are reflected in the release kinetics of 5-FU from the MIL-100 host, in which the stronger guest–host interactions of the manually ground system led to a slower release of the 5-FU drug. Finally, we found that while the vortex grinding approach demonstrated is very effective for the fabrication of pristine MIL-100 (Fe), a manual grinding/milling route yields the enhanced incorporation of drug guest molecules in the MOF pores. Nevertheless, we acknowledge the limitations underlying the reproducibility of the manual grinding approach. The reported findings serve as a proof of concept, to illustrate how different mechanochemical environments can give significantly different outcomes in the quest of fabricating a drug@MOF composite system. Crucially, one should appreciate the complexity underpinning the mechanochemical route, where a deeper understanding of the mechanism of incorporation and the role of mechanical stresses (*e.g.* shear, collision impact, viscous response) are warranted to precisely control the capture of drugs and other large guest molecules.

Conflicts of interest

There are no conflicts to declare.

Acknowledgements

B. E. S. thanks the Minas Gerais Research Foundation (FAPEMIG CNPJ n21.949.888/0001-83) for a DPhil scholarship award. J. C. T. thanks the ERC Consolidator Grant under the grant agreement 771575 (PROMOFS) for research funding. We thank Professor Ronald Roy and Dr Jason Raymond in the Department of Engineering Science, University of Oxford, for



access to the UV-vis spectrometer. We thank the Research Complex at Harwell (RCAH) for access to the TGA-Q50 and the Nicolet iS10 FTIR spectrometer. We are grateful to Dr James Taylor at the STFC ISIS Neutron and Muon Source for performing the nitrogen adsorption measurements.

Notes and references

- (a) M. Rubio-Martinez, C. Avci-Camur, A. W. Thornton, I. Imaz, D. Maspoch and M. R. Hill, *Chem. Soc. Rev.*, 2017, **46**, 3453–3480; (b) C. Mottillo and T. Friscic, *Molecules*, 2017, **22**(1), 144.
- (a) B. E. Souza, S. Rudic, K. Titov, A. S. Babal, J. D. Taylor and J. C. Tan, *Chem. Commun.*, 2019, **55**, 3868–3871; (b) C. Orellana-Tavra, E. F. Baxter, T. Tian, T. D. Bennett, N. K. H. Slater, A. K. Cheetham and D. Fairen-Jimenez, *Chem. Commun.*, 2015, **51**, 13878–13881.
- (a) D. Crawford, J. Casaban, R. Haydon, N. Giri, T. McNally and S. L. James, *Chem. Sci.*, 2015, **6**, 1645–1649; (b) M. Samal, J. Panda, B. P. Biswal and R. Sahu, *CrystEngComm*, 2018, **20**, 2486–2490; (c) M. Bellusci, P. Guglielmi, A. Masi, F. Padella, G. Singh, N. Yaacoub, D. Peddis and D. Secci, *Inorg. Chem.*, 2018, **57**, 1806–1814; (d) M. Piloni, F. Padella, G. Ennas, S. Lai, M. Bellusci, E. Rombi, F. Sini, M. Pentimalli, C. Delitala, A. Scano, V. Cabras and I. Ferino, *Microporous Mesoporous Mater.*, 2015, **213**, 14–21.
- (a) S. L. James, C. J. Adams, C. Bolm, D. Braga, P. Collier, T. Friscic, F. Grepioni, K. D. M. Harris, G. Hyett, W. Jones, A. Krebs, J. Mack, L. Maini, A. G. Orpen, I. P. Parkin, W. C. Shearouse, J. W. Steed and D. C. Waddell, *Chem. Soc. Rev.*, 2012, **41**, 413–447; (b) P. Horcajada, S. Surble, C. Serre, D. Y. Hong, Y. K. Seo, J. S. Chang, J. M. Greneche, I. Margiolaki and G. Férey, *Chem. Commun.*, 2007, 2820–2822; (c) J. Nawrocki, D. Prochowicz, A. Wisniewski, I. Justyniak, P. Gos and J. Lewinski, *Eur. J. Inorg. Chem.*, 2020, **2020**, 796–800.
- (a) A. García Márquez, A. Demessence, A. E. Platero-Prats, D. Heurtaux, P. Horcajada, C. Serre, J.-S. Chang, G. Férey, V. A. de la Peña-O'Shea, C. Boissière, D. Grosso and C. Sanchez, *Eur. J. Inorg. Chem.*, 2012, **2012**, 5165–5174; (b) B. E. Souza, L. Dona, K. Titov, P. Bruzzese, Z. Zeng, Y. Zhang, A. S. Babal, A. F. Moslein, M. D. Frogley, M. Wolna, G. Cinque, B. Civalieri and J. C. Tan, *ACS Appl. Mater. Interfaces*, 2020, **12**, 5147–5156.
- D. Cunha, M. Ben Yahia, S. Hall, S. R. Miller, H. Chevreau, E. Elkaïm, G. Maurin, P. Horcajada and C. Serre, *Chem. Mater.*, 2013, **25**, 2767–2776.
- J. Hou, C. Li, L. Cheng, S. Guo, Y. Zhang and T. Tang, *Drug Dev. Ind. Pharm.*, 2011, **37**, 1068–1075.
- B. E. Souza, A. F. Möslin, K. Titov, J. D. Taylor, S. Rudić and J.-C. Tan, *ACS Sustainable Chem. Eng.*, 2020, **8**, 8247–8255.
- J. Stojakovic, B. S. Farris and L. R. MacGillivray, *Chem. Commun.*, 2012, **48**, 7958–7960.
- L. Han, H. Qi, D. Zhang, G. Ye, W. Zhou, C. M. Hou, W. Xu and Y. Y. Sun, *New J. Chem.*, 2017, **41**, 13504–13509.
- R. Anand, F. Borghi, F. Manoli, I. Manet, V. Agostoni, P. Reschiglian, R. Gref and S. Monti, *J. Phys. Chem. B*, 2014, **118**, 8532–8539.
- R. Kuroda, J. Yoshida, A. Nakamura and S. Nishikiori, *CrystEngComm*, 2009, **11**, 427–432.
- H. Lv, H. Zhao, T. Cao, L. Qian, Y. Wang and G. Zhao, *J. Mol. Catal. A: Chem.*, 2015, **400**, 81–89.
- (a) J. Yang, X. Feng, G. Lu, Y. Li, C. Mao, Z. Wen and W. Yuan, *Dalton Trans.*, 2018, **47**, 5065–5071; (b) M. Klimakow, P. Klobes, A. F. Thünemann, K. Rademann and F. Emmerling, *Chem. Mater.*, 2010, **22**, 5216–5221.

